FULL PAPER

Performance and Stability Enhancement of Dye-Sensitized and Perovskite Solar Cells by Al Doping of TiO_2

Sandeep K. Pathak, A. Abate, P. Ruckdeschel, B. Roose, Karl C. Gödel, Yana Vaynzof, Aditya Santhala, Shun-Ichiro Watanabe, Derek J. Hollman, Nakita Noel, Alessandro Sepe, Ullrich Wiesner, Richard Friend, Henry J. Snaith, and Ullrich Steiner**

Reversible photo-induced performance deterioration is observed in mesoporous TiO_2-containing devices in an inert environment. This phenomenon is correlated with the activation of deep trap sites due to astoichiometry of the metal oxide. Interestingly, in air, these defects can be passivated by oxygen adsorption. These results show that the doping of TiO_2 with aluminium has a striking impact upon the density of sub-gap states and enhances the conductivity by orders of magnitude. Dye-sensitized and perovskite solar cells employing Al-doped TiO_2 have increased device efficiencies and significantly enhanced operational device stability in inert atmospheres. This performance and stability enhancement is attributed to the substitutional incorporation of Al in the anatase lattice, "permanently" passivating electronic trap sites in the bulk and at the surface of the TiO_2.

1. Introduction

The commercial viability of a photovoltaic technology replacing single-crystal silicon solar cells relies on three essential attributes: cost, performance and lifetime. While dye-sensitized and more recently perovskite solar cell are highly promising in terms of the first two attributes, the stability of these devices remains unproven.[1–3]

For solid-state dye sensitized (ssDSSC)[4] and perovskite sensitized solar cells (PSSC)[5] non-stoichiometry induced defects in TiO_2 appears to be a limiting factor for two of the key parameters; efficiency and more importantly the long-term photo-stability. Limitation in charge transport is an important factor for device performance, which has been studied extensively in context of ssDSSCs. Recently the emergence of perovskite-based solar cells (PSSCs) has led to a marked increase in solid-state device performance, to up to 15%. In the perovskite devices, replacing the electron acceptor TiO_2 with an insulating alumina scaffold has played an important part in the increase in open-circuit voltage.[1] This has been rationalized by the presence of deep electron traps in the non-stoichiometric TiO_2 reducing the splitting of the quasi Fermi levels under illumination. The same mechanism is likely to affect ssDSSCs, but in contrast to perovskite solar cells in which organometal trihalide perovskites are a light absorbing charge transporter, ssDSSCs rely on the metal oxide for charge transport, ruling out the use of alumina or other insulating scaffolds.[1]

In ssDSSCs, the dye is regenerated from its oxidised state within a few hundred picoseconds, orders of magnitude faster than in the iodide/triiodide-based liquid electrolyte cells, where dye regeneration occurs on the microsecond time scale.[6] These extremely rapid regeneration dynamics should play an important role in improved long-term stability of the dye in the ssDSSC, since the dye is most likely to degrade in its charged oxidized state.[7] However, to realize long-term stability of DSSCs it is paramount to protect the organic components of the device from oxidation by oxygen, moisture and other oxidizing agents, by encapsulation in inert environment. We have discovered a critical instability of mesoporous TiO_2 based devices; when they are encapsulated in an inert atmosphere and exposed to sunlight, a quick loss in device performance is observed.[8,9] Encouragingly though, the cells recuperate to their initial performance when the encapsulation is broken, exposing them to air.

Here, we discuss in detail the nature of the titania surface chemistry in the presence of oxygen and light, and its role in

Dr. S. K. Pathak, P. Ruckdeschel, B. Roose, K. C. Gödel, Dr. Y. Vaynzof, A. Santhala, Dr. S.-I. Watanabe, Dr. A. Sepe, Prof. R. H. Friend, Prof. U. Steiner
Cavendish Laboratory
Department of Physics
University of Cambridge
JJ Thomson Avenue CB3 0HE, UK
E-mail: ullrich.steiner@unifr.ch
Dr. S. K. Pathak, Dr. A. Abate, D. J. Hollman, N. Noel, Prof. H. J. Snaith
Clarendon Laboratory
Department of Physics
University of Oxford
Parks road, Oxford OX1 3PU, UK
E-mail: h.snaith1@physics.ox.ac.uk
Prof. U. Wiesner
Material Science and Engineering
University of Cornell
214 Bard Hall, Ithaca, NY 14853-1501, USA
Prof. U. Steiner
Adolphe Merkle Institute
Chemin des Verdiers
CH-1700, Fribourg, Switzerland

DOI: 10.1002/adfm.201401658

device performance and stability. In particular, we demonstrate the reversible deterioration of ss-DSSC device performance when exposed to sunlight in an inert atmosphere. We show that this deterioration is primarily caused by oxygen-induced defects in TiO_2 and we postulate that it is driven by photo-induced desorption of adsorbed oxygen. This effect is very effectively suppressed by doping the mesoporous TiO_2, or compact TiO_2 films employed in perovskite cells, with aluminum cations, which have the unexpected benefit of increasing the conductivity of the TiO_2 by many orders of magnitude. Our methodology differs from the various previously employed Al-doping techniques, the role of which in device performance has remained unclear.[10–17]

2. Results

2.1. Reversible Photodegradation of Encapsulated ssDSSCs

We start by examining the stability of ssDSSCs. TiO_2 photoanodes were manufactured using the well-established co-assembly of a polyisoprene-block-polyethyleneoxide (PI-b-PEO) diblock copolymer with a precursor-sol, yielding a mesoporous scaffold.[18,19] In contrast to other methods, this technique provides simultaneous control over the TiO_2 chemistry and meso-structure, which is governed by the self-assembly of the amphiphilic block-copolymer. D102 dye and spiro-MeOTAD were used as a light absorber and hole-conductor respectively. Devices were aged under continuous illumination with simulated AM 1.5 sun light (76.5 $mWcm^{-2}$) and current voltage (J–V) curves were recorded continuously in a sealed ageing box where the atmosphere could be switched from inert to air and vice versa. The temporal evolution of solar cell performance for devices aged in air and an inert atmosphere are shown in **Figure 1**a. Surprisingly, the performance of the latter deteriorated rapidly to approximately half the initial performance within 1 h and in less than 15 h the device became predominantly non-functional. In contrast, the devices aged under ambient conditions lost only ≈5% of their peak power conversion efficiency, which was 10% higher than their initial performance, even after ageing for 15 h.

Interestingly, the non-functional aged devices fully recuperate to their initial performance once the photoactive layer was re-exposed to air, as shown in Figure 1b. The reversible device deterioration of devices aged in an inert atmosphere points to a reversible change in the electronic properties of the device and not to the photo-degradation of the dye or the hole conductor. Irreversible photo-degradation of the organic components is observed only when the device is exposed to light and air for long periods of time.[6,20]

It is unlikely that the hole transporting material (HTM) plays a role in such a rapid and reversible deterioration. In a recent publication we have shown that oxygen and light are required to oxidize spiro-MeOTAD, but in the presence of LiTFSI such oxidation is irreversible and its reduction is unlikely during the ageing process.[21,22] The argument that the degradation of the sealed device performance does not arise from the HTM is confirmed in a separate study in which we replaced Spiro-MeOTAD with poly(3-hexylthiophene) (P3HT), as shown in Figure S1. The resulting DSSCs behaved similar to Spiro-MeOTAD-based devices when aged under similar conditions.[8] In difference to Spiro-MeOTAD, neat P3HT is sufficiently conducting and does not need to be oxidized before use.[23,24]

We also show normalized solar cell performance during continuous ageing at room temperature (RT) for encapsulated (which resembles an inert atmosphere), and non-encapsulated ssDSSCs for a longer period of time, see Figure S2a. Figure S2b shows the UV-vis spectra of dye molecules adsorbed on TiO_2, encapsulated and non-encapsulated, at RT. This demonstrates that dye molecules are stable when encapsulated; in contrast non-encapsulated films are completely degraded after several hours of ageing. The encapsulated films show quite a remarkable resistance to thermal degradation even at elevated temperatures, 100 and 120 °C, as shown in Figure S2c.

Since neither dye degradation, nor changes in the HTM appear to be responsible for the marked loss in device performance, it is necessary to investigate the electronic properties of the TiO_2 meso-structure during illumination in an inert atmosphere. A close look at the current and voltage decay of sealed devices in Figure 1b shows a rapid drop in the open-circuit voltage and in short-circuit current. The former is indicative of the formation of low-resistance electrical pathways across the device, while the latter may either be caused by a rapid acceleration of electron hole- recombination[25,26] or the introduction of deep electron traps, from which the electrons cannot escape, leading to direct recombination with holes. The formation of energetically deep traps in TiO_2 nanocrystals has been reported to be induced by UV light.[27] Our results indicate that these traps interact with the oxygen in air, as explained below.

This gives rise to a conundrum in device design: sealed devices are required to prevent the oxidation of dye and HTM, while the presence of oxygen passivates electron traps in TiO_2.

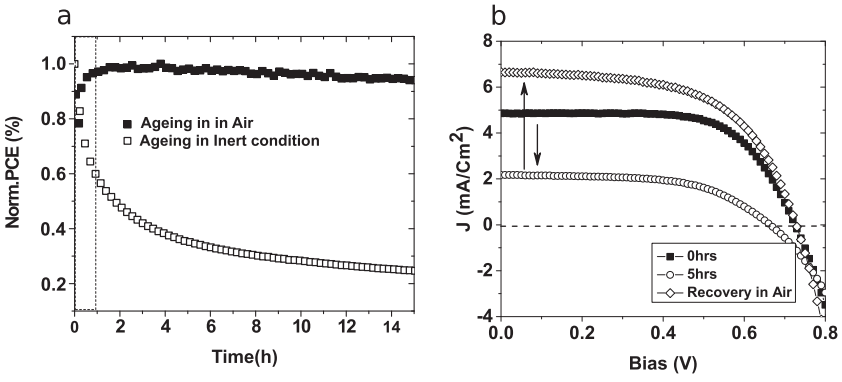

Figure 1. Ageing of ssDSSCs. (a) Normalized performance of ssDSSCs during continuous illumination in air and in an inert atmosphere. The former shows a very small gradual performance degradation whereas the latter shows substantial rapid deterioration within an hour. (b) J–V curves of a device that was first aged in inert atmosphere and then exposed to air exhibiting more-than full recovery of the initial device performance.

Addressing trap formation in TiO_2 is the only way to solve this dilemma.

2.2. Alumina-Modified TiO_2 Photoanodes

To address the implications of defect states in TiO_2 crystals we have investigated doping of TiO_2 with a number of different ions. Titanium is tetra-valant, and will usually be doped with penta (or greater) valent ions to induce n-type doping and ions with a lower valancy to induce p-type doping. We found a remarkable impact of doping TiO_2 with tri-valent aluminum. The advantage of synthesising mesoporous TiO_2 photoanodes by block-copolymer directed sol-gel chemistry is the ease of chemical modification. Here, we have added an Al-containing precursor to the Ti-sol in a well-controlled fashion to substitutionally dope the resulting anatase TiO_2.

Figure 2a shows scanning electron microscopy (SEM) and atomic force microscopy (AFM, inset) images of a meso-structured TiO_2 films, synthesized with 1% Al precursor. The well-defined pore-morphology arises from the self-assembly of the block-copolymer, which is removed by high temperature sintering.[28] The formation of smooth films with the 20 nm meso-morphology is invariant with the addition of the Al-containing precursor, indicating the robustness of this processing method with respect to changes in the employed sol-gel chemistry.

The TiO_2 lattice structure was confirmed by X-ray diffraction (XRD) of pristine TiO_2 and films manufactured with added Al-precursor (Figure 2b). All peaks can be assigned to the anatase phase of TiO_2, indicating that anatase nano-crystalline structure is retained upon Al precursor addition of up to 5 mol%. No Al_2O_3 peaks were observed even for the highest (5 mol%) doping concentration.

While the (101) anatase peak exhibited a slight shift towards 2θ for the two higher doping levels (2.5 and 5 mol%), the peak positions of low-level doped TiO_2 (0.5 and 1 mol%) did not show any discernible difference to pure anatase. An increase in the broadening of the (101) anatase peak with increasing doping was observed for all Al concentrations. The TiO_2 crystallite size was calculated using Scherrer equation, which reduces with the increasing doping concentration,[10] as shown in Figure S3.

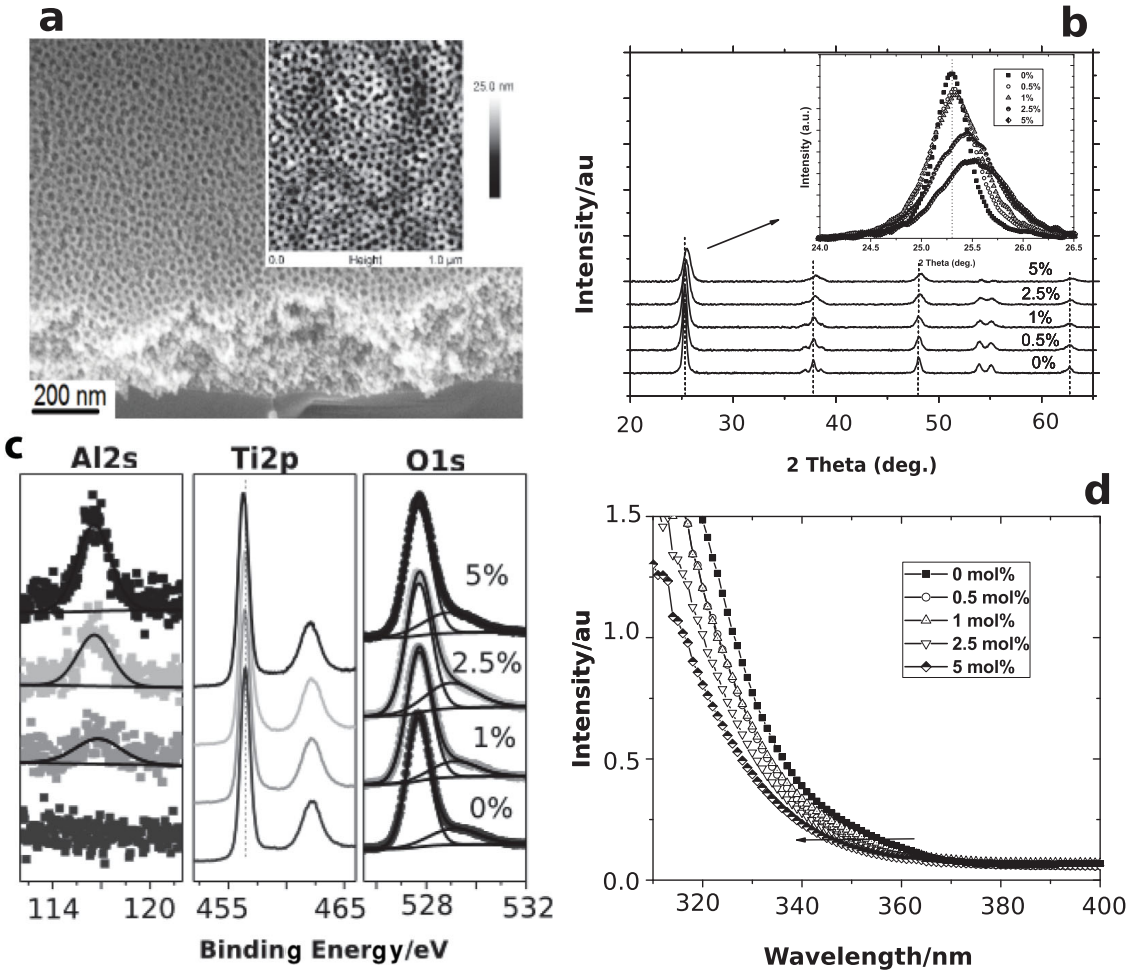

Figure 2. Al-doped mesostructured TiO_2 films. (a) SEM and AFM (inset) images of the 20-nm morphology that arises from PI-b-PEO self-assembly. (b) XRD (101), (211) and (105) TiO_2 peaks show only a slight shift towards lower 2θ values. (c) XPS, and (d) UV-vis spectra of the TiO_2 meso-structure for varying doping concentrations, indicating a blue shift with the Al doping.

Low doping concentrations (0.5 and 1 mol%) only introduce a small amount of impurities, mostly as point defects in the crystal. The lattice parameter is unchanged and so are the XRD peaks. An increase in the doping concentration (2.5 and 5 mol%) may introduce stresses in the lattice, resulting in peak shifts.[29] The small peak shifts are in agreement with the relatively small difference in ionic radii of Al(III) (0.53 nm), Ti(IV) (0.61 nm) and Ti(III) (0.64 nm), resulting in only a small distortion of the anatase lattice upon Al-doping.[4]

Al-doping was further corroborated by X-ray photoemission spectroscopy (XPS). Figure 2c shows XPS spectra of Al2s, Ti2p and O1s for doped and undoped samples. The Al2s peak increases in peak intensity with increasing dopant concentration. The calculations of the Ti to Al atomic ratios based on XPS for different doping levels was: 1% – (14.57), 2.5% –(9.16) and for 5% – (5.73).

The binding energies of Ti in the anatase lattice at 458.8 and 464.5 eV correspond to Ti2p 3/2 and Ti2p 1/2 respectively. The Ti2p and Al2s core level spectra of the Al doped films show only one single component. The O1s major component near a binding energy of 530.0 eV may correspond to bonding with Ti and Al. The other component near the binding energy of 531.4. eV may mainly correspond to hydrated bonds or carbonate caused by contaminations on the film surface.[13] For the highest Al doping of 5 mol%, the Ti2p peak was shifted to a lower binding energy (by 0.4 eV). This shift by the Al doping is due to a charge transfer effect, suggesting that the Al ions are incorporated in the TiO_2 lattice and do not form a separate phase.[30]

The UV-vis absorption spectra in Figure 2d show an incremental blue shift with Al-doping, as also shown by previous authors.[11,31] A blue shift indicates a possible increase in the effective band gap, where the Fermi level moves closer to the conduction band. An increase in the band gap further corroborates Al (III) doping into the TiO_2 crystal lattice. A widening of band gap due to quantum confinement can be ruled out since the crystal sizes for doped and undoped TiO_2 are larger than 10 nm (see Figure S3).[32,33]

We have investigated the electron conductivity of the undoped and doped TiO_2 meso-structured films by performing space charge limited current (SCLC) measurements,[34] shown in **Figure 3**a. For undoped TiO_2, the quadratic dependence of current with the voltage indicates the existence of space charges, e.g. oxygen vacancies, Ti interstitials, Ti(III), etc. For low concentrations of Al-doping (0.5 and 1 mol%) the current-voltage (J–V) curves are linear, indicating velocity-saturated conduction (i.e. a suppression of space charges) and a substantial conductivity enhancement. Upon a further increase in doping (2.5, 5 mol%), the ohmic character of the J–V curves is maintained but the conductivity is substantially reduced. This indicates a suppression of charged defects, but excess Al^{3+} may act as scattering centers for charges and hence reduce the conductivity. It suffices to say that up to certain concentration, Al^{3+} doping reduces the defects density. To further corroborate this and to investigate the sub-band gap density of states by Al doping photo-thermal deflection spectroscopy (PDS) was carried out, as shown in Figure 3b. Sub-bandgap optical absorption can be used to characterize band-tail states induced by disorder in the anatase crystal.

This sub-bandgap absorption tail has an exponential variation, $A \sim \exp(E/E_u)$, defining the Urbach Energy E_u which is a measure for the degree of disorder within the material.[35,36] The inset in Figure 3b shows a decrease in E_u upon 0.5 mol% Al-doping followed by an increase for higher Al concentrations. For 2.5 and 5 mol% doping the Urbach energy is even higher than in undoped TiO_2. This is further evidence that Al doping reduces the number of trap states for low concentration doping (0.5 and 1 mol%). E_u follows a similar trend as the conductivity.

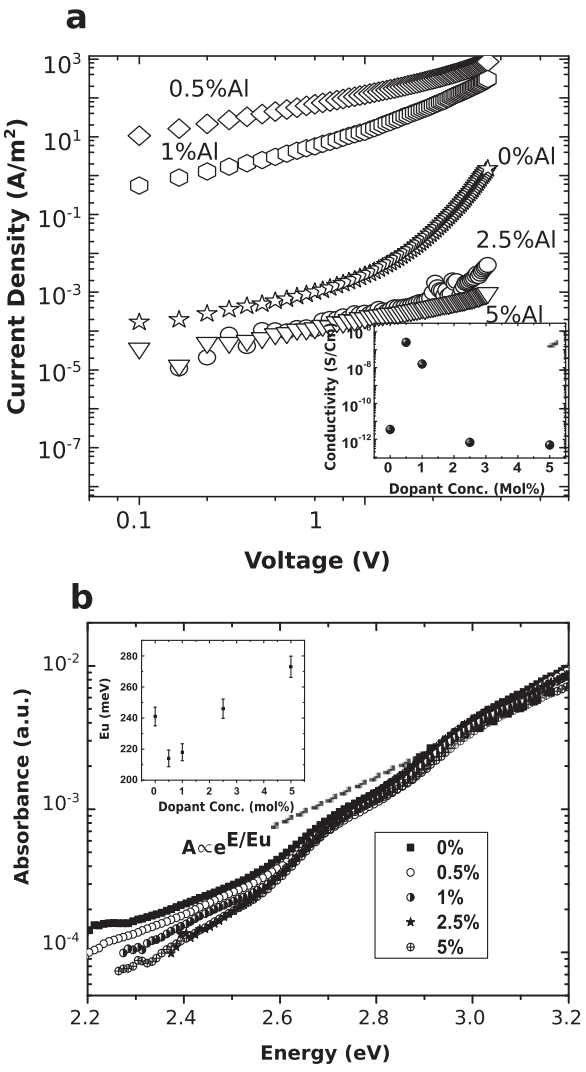

Figure 3. Enhancement of charge carrier conductivity and reduction of defect states with Al-doping. (a) Current-voltage curves for un-doped and doped TiO_2 mesostructured thin films under an inert atmosphere. The inset shows the electron conductivity derived from SCLC measurements, (b) PDS spectra for different dopant concentrations. The inset shows the corresponding Urbach energies.

2.3. ssDSSCs Based on Al-Doped TiO_2

Oxygen defects in the metal oxide photoanode have a direct impact on solar cell performance. Their removal should enhance the device efficiency. To investigate if this is the case,

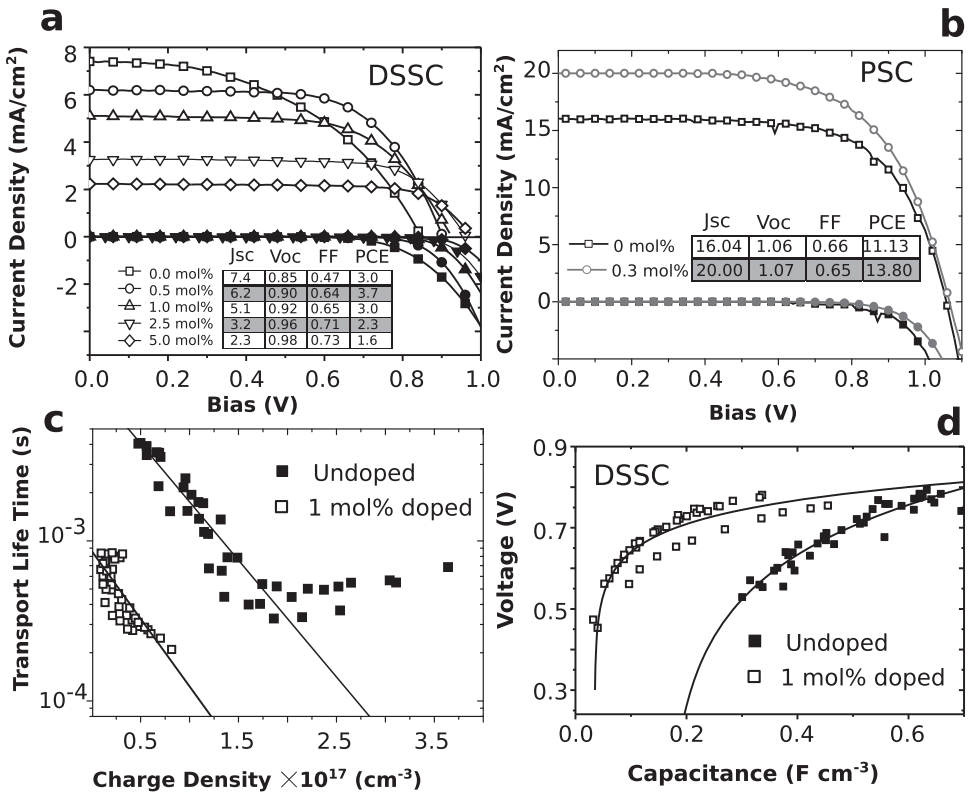

Figure 4. Electronic properties of Al-doped solar cells. *J–V* curves recorded under AM 1.5 simulated sun light (100 mW cm^{-2}); the respective dark currents are also shown. (a) ssDSSCs fabricated with doped and undoped meso-structured TiO_2. (b) PSCs manufactured with doped and undoped solid flat TiO_2 hole blocking layers. The device performance parameters are summarized in the inset-tables. (c) ssDSSC charge transport lifetimes at short circuit vs. charge density. (d) ssDSSC differential capacitance vs. open circuit voltage. The lines in (c) and (d) are single-exponential fits.

ssDSSCs and perovskite based MSSCs were manufactured with Al-doped meso-structured TiO_2 (DSSCs) and compact TiO_2 for the n-type selective contact in MSSCs. The *J-V* curves of these devices are shown in **Figure 4**a,b. For ssDSSCs a clear trend emerges. A continuous increase in open circuit voltage (V_{oc}) and fill-factor (*FF*) and a continuous decrease in short circuit current (J_{sc}) is observed with increasing Al-doping levels. For the lowest doping concentration the marked increase in V_{oc} and *FF* resulted in the highest power conversion efficiency (PCE). Both the increase in V_{oc} and the decrease in J_{sc} with Al-doping may be correlated with an increase in the TiO_2 conduction band (CB) (10 to 50 meV upon doping from 0.5 to 5%, as indicated by the UV-vis spectra). The negative impact of the increase in the TiO_2 CB is that it may reduce the charge injection efficiency from the dye into TiO_2.[37–40] A similar effect was found for chemically treated TiO_2.[41] The reduction in J_{sc} is however quite large for the relatively small CB-shift upon Al-doping. This has been explained with an enhancement of doping density at the crystal surface, causing a locally enhanced CB-shift that substantially reduces charge injection.[42,43] The possibility of higher Al-doping densities at the crystal surface has been reported before,[42,43] presumably arising from the higher number of oxygen vacancies at the surface combined with the ability of Al (III) to diffuse within the crystal.[42,44] The raise in V_{oc} of over 100 mV for the highest doping concentration is, on the other hand, larger than the maximum CB-shift of 50 meV indicated by the UV-vis measurements. However, the UV-vis measurements show a general widening of the bandgap, but do not specify if there is any preferential shift in the conduction or valence band, nor are they sensitive to any change in surface potential, which may arise from a change in surface charge.

We have further investigated the impact of Al doping by performing small perturbation photo-voltage and photocurrent decay measurements on the dye-sensitized solar cells.[45] These measurements can be used to extract charge collection lifetimes (how fast charges diffuse out of the solar cell), charge recombination lifetimes, and also determine the differential capacitance as a function of open-circuit voltage which is closely related to the density and position of sub-bandgap states in TiO_2. Figure 4c shows the charge collection lifetime for Al doped and pristine TiO_2 based DSSCs. We observe that, for the same charge density, there is a significant increase of more than one order of magnitude in transport rate for Al doped DSSCs. This is consistent with the enhanced conductivity determined by SCLC measurements.

Figure 4d shows the differential capacitance-voltage curve, which clearly illustrates a substantial reduction in the sub-band gap density of states for the Al doped TiO_2. This is in good agreement with the PDS and UV-Vis absorption analysis (Figures 3b and 2d). At higher charge densities, the capacitances converge, but the Al doped material exhibits a significantly

reduced capacitance at low voltages, consistent with the passivation or elimination of sub-band gap states.

2.4. Perovskite MSSCs with Al-Doped TiO_2 Compact Layers

Perovskite-based meso-superstructured solar cells eliminate the requirement for mesoporous TiO_2, since this is replaced with a mesoporous insulating scaffold, typically Al_2O_3, and the perovskite absorber assumes the roles of light absorption and long range charge transport. However, in the current most efficient embodiment, a flat compact layer of TiO_2 of about 50 nm is still employed as the electron selective contact forming a planar heterojunction with the perovskite film.[1] We have produced 50 nm thick TiO_2 compact layers using the sol-gel chemistry discussed above, in the absence of the block-co-polymer structure-directing agent, with various Al-doping levels. Samples with Al concentrations of 0.5, 1, 2.5 and 5 mol% were prepared and MSSCs were fabricated as discussed elsewhere.[1,46] The mesoporous alumina thickness was 400 nm and the mixed halide perovskite precursor was cast with a 3:1 molar ratio of CH_3NH_3I:$PbCl_2$ at 40 wt% in DMF.

The solar cell performance parameters of this series are shown in the Supplementary Information (Figure S4). The V_{oc} for the chosen doping range i.e. 0.5, 1, 2.5 and 5 mol%, shows an incremental improvement, but the overall PCE values do not show any improvement as compared with the undoped device, possibly due to a reduction in J_{sc} (which is partially offset by a V_{oc} increase). Further optimization led to a lowering of doping levels to i.e. 0.3 mol%. The *J–V* curve of the best performing device is shown in Figure 4b. Devices using this doping level (0.3 mol%) showed an enhanced J_{sc} value, leading to an improved device efficiency of 13.8%, compared with a pristine compact layer which had a PCE of 11.1%. This is most likely connected to the improved conductivity of TiO_2 for low Al-doping.

3. Discussion

3.1. Lattice Defects in TiO_2

The sensitivity of ssDSSCs to the presence of oxygen and Al-doping points to the importance of lattice defects in anatase. There is a general consensus that oxygen vacancies and/or Ti interstitials are the predominant reason for non-stoichiometry in TiO_2, arising form the reduction of Ti(IV) to Ti(III).[47–50] The removal of one neutral oxygen atom from the lattice leaves one point defect and two under-coordinated Ti(III) (**Figure 5**a). Since Ti(III) is less stable then Ti(IV) it acts as an electron trap, forming $Ti(IV)^+ + e^-$. In anatase crystals, TI(III) defects induce a shallow energy level (0.7–1 eV) below the conduction band which is not easily available for electron transport and act as an electron trap sites. Because of its unsaturated coordination, Ti(III) is reactive. When reacting with oxygen, the thermodynamically stable O_2^- superoxide is formed, which is Coulomb-bound to the positively charged $Ti(IV)^+$ to form a $Ti(IV)^+ - O_2^-$ complex (Figure 5c).

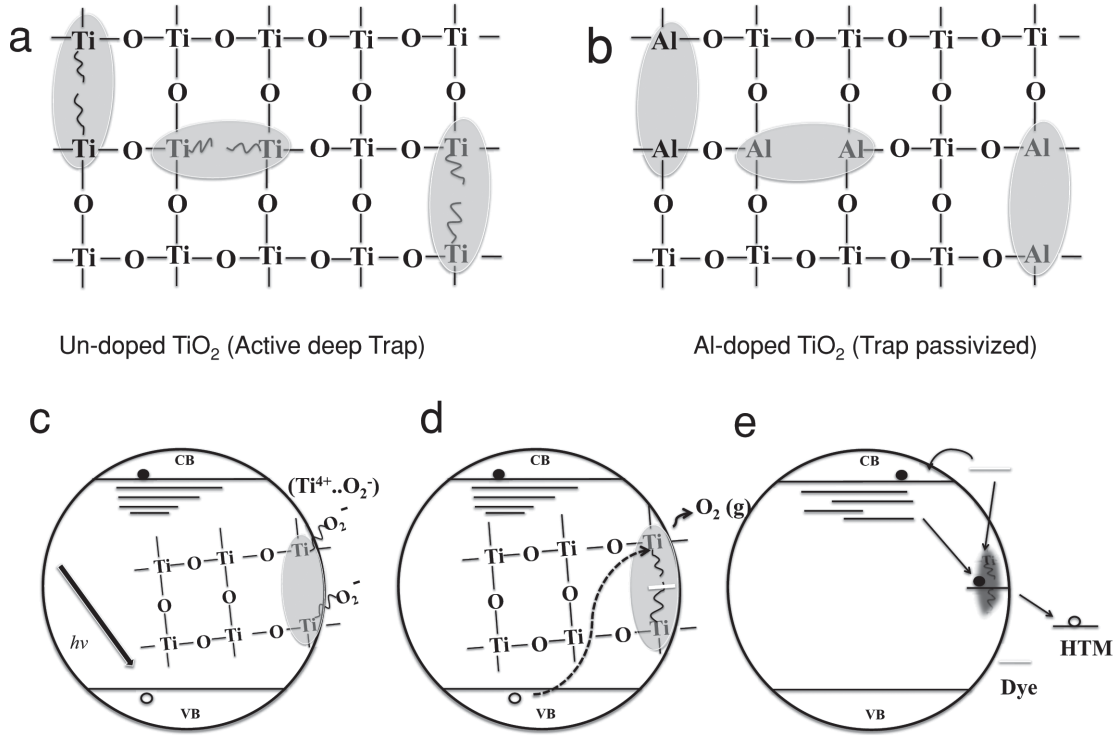

Figure 5. Schematic of Ti(III) trap passivation, doping and oxygen adsorption. (a) Oxygen defects in the lattice give rise to Ti(III) defects that form deep electronic traps. (b) Al substitution at the Ti(III) sites passivates these defects. (c) In the presence of oxygen, ionisation of Ti(III) gives rise to O_2^- superoxide which passivates the trap sites. (d) Photoexcited holes neutralise and desorb O_2, activating Ti(III), which (e) enables charge recombination.

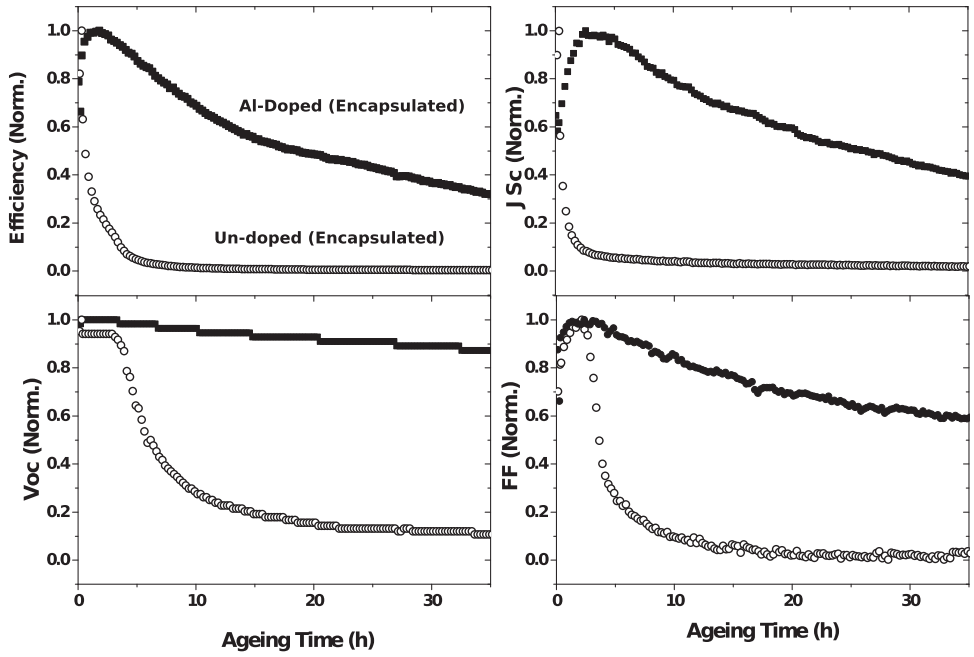

Figure 6. Ageing of ssDSSCs. Normalized solar cell performance parameters during ageing, in inert atmosphere, of ssDSSCs fabricated with undoped and 2.5 mol% Al-doped mesostructured TiO_2.

This complex is stable and does not significantly distort the CB, thereby effectively passivating the Ti(III) electron trap. This O_2 adsorption occurs predominantly at surface oxygen defects.[51–53]

UV photo-exitation forms an electron-hole pair in TiO_2. The hole in the valence band recombines with the unpaired O_2^- electron, setting free a neutral oxygen molecule[27,54] (**Figure 6**d). This reverts the $Ti(IV)^+ - O_2^-$ complex to Ti(III), generating deep defect levels. These deep energy levels provide a cascading path for the recombination of injected electrons in the CB of TiO_2 with holes in Spiro-MeOTAD[55–57] (Figure 5e). In the presence of air, the $Ti(IV)^+ - O_2^-$ complexes are able to re-form, while in oxygen-free encapsulated devices these complexes are depleted and the population of deep electronic traps increases, enhancing the recombination rate to a point where the device becomes non-functional within a few hours.

3.2. The Role of Al Doping

Despite a lack of agreement on the effect of Al-doping of TiO_2, Al was found to occupy Ti substitution sites,[44,58–61] interstitial sites,[62,63] a combination of both,[64] and a combination of Ti substitution and oxygen vacancies.[63,65] Our results are best described by the latter result, which is also believed to be thermodynamically favorable.[66]

In contrast to Ti(III), Al(III) is the most stable form of Al, while having a very similar ionic radius as Ti(IV) and Ti(III). The substitution of Al(III) for Ti(IV) is energetically unfavourable[66] and would lower the anatase band-gap, in contrast to our observation. The substitution of two Ti(IV) with Al(III) and the release of the bridging oxygen was however reported to be thermodynamically and electronically more favorable than the creation of a lone oxygen vacancy,[66] which in essence corresponds to the substitution of the two adjacent Ti(III) of an oxygen vacancy. Al(III) substitution therefore removes oxygen defects from the lattice (Figure 5b). This type of Al(III) substitutional doping combined with oxygen vacancies does not introduce defect energy levels in the band gap because of the stable 3-fold coordination of Al(III). The presence of Al(III) raises the CB band and widens the band gap, in agreement with our experimental observation.

The substitution of two Ti(III) adjacent to an oxygen defect with two Al(III) is only possible if Al(III) is able to migrate as interstitial ion through the lattice during processing, as confirmed by several studies.[47,66] The reduction in Ti(III) and lone oxygen vacancies also explains the PDS data in Figure 3b. Most importantly, the stability of Al(III) removes the sensitivity of the anatase photo-anode to the presence of oxygen and therefore makes the doped TiO_2 invariant to ageing under irradiation and heat.

3.3. Device Lifetime Improvement

The effect of Al-doping on the recoverable device degradation shown in Figure 1 was tested, using the same ageing procedure described above. The temporal evolution of solar cell performance parameters for devices aged in inert atmosphere is shown in Figure 6.

While the undoped devices degraded significantly over the short measurement period of 30 min in an inert atmosphere, the performance of the 2.5 mol% Al-doped devices was unchanged. This does not amount to a stable solar cell, but indicates that the substantial reduction in sub-band gap density of states caused by Al doping has significantly assisted the reduction of short-term degradation observed for ssDSSCs operating in an inert atmosphere. Experiments over longer ageing times are currently in progress.

4. Conclusions

We have explored the implications of non-stoichiometric defects in TiO_2 on the dye sensitized and perovskite solar cells. Oxygen vacancy induced defects in anatase TiO_2 were identified not only limit electron transport within the material but are also the cause of substantial deterioration of device operation upon UV-irradiation in inert condition. This gives rise to a conundrum: sealed, oxygen-fee devices degenerate rapidly because of the loss of defect-passivating O_2^- under realistic device operation. In unsealed devices, on the other hand, dye oxidation is the cause of permanent losses in device efficiency.

A low level of Al-doping into TiO_2 substantially resolves this problem. Employing mixtures of Ti- and Al-containing precursors in a sol-gel chemical synthesis, and by inducing a 20-nm mesoporous length-scale by block-copolymer self-assembly, we have fabricated mesostructured Al-doped anatase TiO_2. The substitution of Al into the TiO_2 lattice was confirmed by XPS and UV-vis spectroscopy. PDS measurements suggested that Al-doping reduces the number of sub-bandgap states (increasing the V_{oc}) and dramatically increases electron conductivity. This leads to an overall improvement in device performance of dye sensitized and perovskite based meso-superstructured solar cells (which employ a compact TiO_2 n-type collection layer). More importantly, we have observed that low levels of Al-doping reduced the rate of the rapid performance deterioration of encapsulated devices, which occurs for devices based on pristine TiO_2.

Both the improvement in solar cell performance and increase in stability are attributed to the reduction of non-stoichiometric oxygen-induced defects in the TiO_2 by Al-doping, which permanently passivates bulk and surface defects, removes deep electronic traps and sub-bandgap states and raises the conduction band. Importantly, the employed processing technique is simple and scalable. Based on earlier sol-gel approaches, no additional processing steps are introduced and the only alteration is the introduction of an Al- containing precursor sol. Our method is general and robust, and easily adaptable to TiO_2 doping with other metals. This study is a significant step on the path towards the realization of solid-state DSSCs with practical outdoor operational lifetimes.

5. Experimental Section

Substrate Preparation: FTO-coated glass sheets (7/□, Pilkington) were etched with zinc powder and HCl (2 M) to obtain the required electrode pattern. The sheets were then washed with soap (2% Hellmanex in water), deionized water, acetone, and methanol. The last traces of organic residues were removed by oxygen plasma cleaning. The FTO sheets were subsequently coated with a compact layer of TiO_2 (100 nm) by spin-coating a titanium sol precursor at 2000 rpm. The titanium precursor sol was prepared by drop-wise adding a solution of 175 µL Ti isopropoxide in 1.25 mL EtOH into a solution of 17.5 µL of 2 M HCl in 1.25 ml EtOH. The coated FTO substrate was then heated to 300 °C for 30 min.

Mesostructured TiO_2 Electrodes: Meso-structured TiO_2 electrodes were fabricated using a BCP as a structure-directing agent for the condensation reaction of sol-gel chemistries.[67] The polyisoprene-*block*-polyethyleneoxide (PI-*b*-PEO) block-copolymer (BCP) (0.4 g, molecular weight M_n = 34.4 kg mol^{-1}, 28 wt% PEO) was dissolved in 8 ml of an azeotrope solvent (72.84 wt% toluene and 27.16 wt% 1-butanol). Separately, a titanium precursor sol was prepared by adding 1.54 ml titanium (IV) isopropoxide (Sigma Aldrich, 99.999%) to 0.49 ml hydrochloric acid (37%) under vigorous stirring. After stirring for a few minutes, the titanium precursor sol was added to the polymer solution and subsequently stirred for a further 30 min. For Al-doping, 0.5, 1, 2.5 and 5 mol% aluminum isopropoxide pre-cursor was added and stirred until the solution became clear. The resulting solution was spin-coated (2000 rpm, 40 s) onto the compact layer coated FTO substrate. The films were then annealed on a hot-plate (2000 W, Harry Gestigkeit GmbH), typically for 10 min at 50 °C, followed by a 45 min linear heating ramp to 300 °C and held there for 5 min. The procedure of film deposition and subsequent annealing was repeated 3 times to achieve the required layer thickness. Finally, the entire stack was calcinated at 600 °C (3 h, heating ramp 5 °C /min) to remove the organic material and to crystallise the TiO_2.

Compact Layer Doping: The compact layer preparation above was modified by adding 0.3, 0.5, 1, 2.5 and 5 mol% aluminum isopropoxide precursor to the Ti isopropoxide solution.

Materials Characterization: Scanning electron microscopy was carried out on a LEO 1550 FESEM (Zeiss) with a field emission source operated at an acceleration voltages of 5 kV.

X-ray diffraction was measured using Bruker D8 theta/theta (i.e. fixed sample) spectrometer with a position sensitive detector (LynxEye) and a standard detector (SC) with auto-absorber and graphite 2nd beam monochromator (Bragg Brentano parafocusing geometry, reflection mode).

For X-ray photoemission spectroscopy (XPS) measurements, TiO_2 samples were fabricated on an oxide-covered silicon wafer, which was transferred into the ultrahigh vacuum chamber of an ESCALAB 250Xi. The measurements were carried out using a XR6 monochromated Alkα X-ray source ($h\nu$ = 1486.6 eV) with a 650 µm spot size.

To measure conductivity, space charge limited current (SCLC) in a vertical configuration was adopted. 100 nm TiO_2 films were spin-coated on 25 nm gold coated corning 1737F glass substrate (15 mm × 15 mm). A top electrode of 25 nm gold was deposited on top of the film.

Photothermal deflection spectroscopy (PDS) was used to measure sub band gap states in TiO_2 films deposited on Si-substrates. PDS is a highly sensitive surface-averaged absorption measurement technique. For the measurements, the sample was exposed to monochromatic light (pump beam), producing a thermal gradient due to the non-radiative relaxation of the absorbed light. This results in a refractive index gradient in the area surrounding the sample surface, which was further enhanced by immersing the sample in an inert liquid (Fluorinert FC-72) which has high refractive index changes for small variations in temperature. A fixed wavelength continuous wave laser beam (probe beam) (670 nm) was passed through this refractive index gradient producing a deflection proportional to the absorbed light. This deflection was measured using a position sensing detector and a lock-in amplifier. The deflection is proportional to the light absorption in the sample at that wavelength of the pump pulse, and scanning pump-pulse wavelength yields a complete absorption spectrum.

UV-vis absorption was measured on films in air using a commercial spectrophotometer (Varian Cary 300 UV-Vis, USA).

Device Fabrication: For ssDSSC fabrication, mesoporous electrodes were cut down to size and soaked in a $TiCl_4$ aqueous bath (2×10^{-2} M) for 1 hour at 70 °C in an incubator. After rinsing with deionized water and drying in air, the films were heat-treated at 500 °C for 45 min in air, cooled to 70 °C and finally immersed in a 0.5 mM C106 dye solution (in a 1:1 mixture of acetonitrile and tert-butyl alcohol) for 12 h. The dye-adsorbed films were then rinsed with acetonitrile before spinning-on spiro-MeOTAD (LUMTECH) hole-conductor at 1000 rmp for 60 s in air. The solution for spin-coating consisted of spiro-MeOTAD dissolved in anhydrous chlorobenzene (reagent grade) at 10 vol%, assuming a density of spiro-MeOTAD of 1 g cm^{-3}. Tert-butyl pyridine (tbp) was added to the solution at a concentration of 1.26 µL mg^{-1} (tbp: spiro-OMeTAD). Lithium bis(trifluoromethyl sulfonyl)imide salt (Li-TFSI) (170 mg mL^{-1} in acetonitrile) was added. After drying overnight, back contacts were applied by thermal evaporation of 150 nm of silver.

Perovskite solar cells were fabricated on doped and undoped compact TiO_2 layers. An Al_2O_3 meso-structured scaffold was deposited by spin-coating a colloidal dispersion of 20nm Al_2O_3 nanoparticles in isopropanol, followed by drying at 150 °C. Upon cooling to room temperature, a DMF solution of methyl- ammonium iodide and $PbCl_2$ (3:1 molar ratio) was deposited by spin-coating, which forms a perovskite after heating to 100 °C for 45 min. Spiro-MeOTAD and an Ag-electrode were deposited in similar fashion as in the fabrication of ssDSSCs.

For the measurement of the solar-cell device parameters, solar-simulated AM 1.5 sunlight was generated with an ABET solar simulator calibrated to output 100 mW cm^{-2} using an NREL- calibrated KG5 filtered silicon reference cell, and the *J-V* curves were recorded with a Keithley 2400 source meter. The solar cells were masked with a metal aperture defining an active area of 0.09 cm^2. Photovoltage and photocurrent decay measurements were performed by a similar method as O'Regan *et al.*[38,68–70]

The devices were sealed inside a glove box in inert atmosphere. Surlyn (DuPontTM Surlyn packaging resins) were cut to size, placed on the device and a glass slide covering the entire active area was placed over the device. The assembly was placed on hot plate set to 130 °C with the glass slide facing down for several minutes and a uniform pressure was applied. Commercial two-part epoxy resin mixed with the appropriate hardener was then applied around the device to further seal its sides.

Ageing measurements were performed in a SUNTEST CPS+ (Atlas material testing solution) ageing chamber, equipped with a 1500 W air-cooled xenon lamp, (O 76.5 $mWcm^{-2}$). A sample holder was placed inside the chamber, and the sample was connected to the Keithely source meter. The samples were kept inside the chamber for the entire measurement period under constant illumination and fixed temperature and *J–V* -curves were taken every 30 min.

Supporting Information

Supporting Information is available from the Wiley Online Library or from the author.

Acknowledgements

This work was funded by EPSRC, Oxford Photovoltaics Ltd and the EC through the FP7 project SANS.

Received: May 22, 2014
Published online: July 22, 2014

[1] M. M. Lee, J. Teuscher, T. Miyasaka, T. N. Murakami, H. J. Snaith, *Science* **2012**, *338*, 643.
[2] B. G. M. O'regan, *Nature* **1991**, *353*, 737.
[3] A. Kojima, K. Teshima, Y. Shirai, T. Miyasaka, *J. Am. Chem. Soc.* **2009**, *131*, 6050.
[4] U. Bach, D. Lupo, P. Comte, J. E. Moser, F. Weissortel, M. Gra, *Letter to Nature* **1998**, *395*, 583.
[5] H.-S. Kim, C.-R. Lee, J.-H. Im, K.-B. Lee, T. Moehl, A. Marchioro, S.-J. Moon, R. Humphry-Baker, J.-H. Yum, J. E. Moser, M. Grätzel, N.-G. Park, *Sci. Rep.* **2012**, *2*, 591.
[6] F. Nour-Mohhamadi, S. D. Nguyen, G. Boschloo, A. Hagfeldt, T. Lund, *J. Phys. Chem. B* **2005**, *109*, 22413.
[7] N. Kato, Y. Takeda, K. Higuchi, A. Takeichi, E. Sudo, H. Tanaka, T. Motohiro, T. Sano, T. Toyoda, *Sol. Energy Mater. Sol. Cells* **2009**, *93*, 893.
[8] S. K. Pathak, *Adv. Energy Mater.* **2013**, DOI: 10.1002/aenm.201301667.
[9] T. Leijtens, G. Eperon, S. Pathak, A. Abate, M. Lee, H. Snaith, *Nat. Commun.* **2013**, *4*, 2885.
[10] Y. J. Choi, Z. Seeley, A. Bandyopadhyay, S. Bose, S. a. Akbar, *Sens. Actuat. B Chem.* **2007**, *124*, 111.
[11] F. Huang, M. Zhou, Y. Cheng, R. A Caruso, *Chem. Mater.* **2006**, *18*, 5835.
[12] S. K. Kim, G. J. Choi, J. H. Kim, C. S. Hwang, *Chem. Mater.* **2008**, *20*, 3723.
[13] S. K. Kim, G.-J. Choi, S. Y. Lee, M. Seo, S. W. Lee, J. H. Han, H.-S. Ahn, S. Han, C. S. Hwang, *Adv. Mater.* **2008**, *20*, 1429.
[14] S. Liu, G. Liu, Q. Feng, *J. Porous Mater.* **2009**, *17*, 197.
[15] C.-Y. Tsai, H.-C. Hsi, H. Bai, K.-S. Fan, H.-D. Sun, *Jpn. J. Appl. Phys.* **2012**, *51*, 01AL01.
[16] K. H. Kim, K. Utashiro, Z. Jin, Y. Abe, M. Kawamura, *Int. J. Electrochem. Sci.* **2013**, *8*, 5183.
[17] H. Alarcón, G. Boschloo, P. Mendoza, J. L. Solis, A. Hagfeldt, *J. Phys. Chem. B* **2005**, *109*, 18483.
[18] J. Lee, M. C. Orilall, S. C. Warren, M. Kamperman, F. J. DiSalvo, U. Wiesner, *Nat. Mater.* **2008**, *7*, 222.
[19] P. F. W. Simon, R. Ulrich, H. W. Spiess, U. Wiesner, *Chem. Mater.* **2001**, *13*, 3464.
[20] G. Xue, Y. Guo, T. Yu, J. Guan, X. Yu, *Int. J. Electrochem. Sci* **2012**, *7*, 1496.
[21] Y. Kim, Y.-E. Sung, J.-B. Xia, M. Lira-Cantu, N. Masaki, S. Yanagida, *J. Photochem. Photobiol. A Chem.* **2008**, *193*, 77.
[22] Y. Saito, *Electrochem. Commun.* **2004**, *6*, 71.
[23] A. Guerrero, P. P. Boix, L. F. Marchesi, T. Ripolles-Sanchis, E. C. Pereira, G. Garcia-Belmonte, *Sol. Energy Mater. Sol. Cells* **2012**, *100*, 185.
[24] H. Hintz, H. Peisert, H. Egelhaaf, T. Chass, *J. Phys. Chem. C* **2011**, *115*, 13373.
[25] H. Al-Dmour, D. M. Taylor, *Appl. Phys. Lett.* **2009**, *94*, 223309.
[26] M. Lira-Cantu, K. Norrman, J. W. Andreasen, N. Casan-Pastor, F. C. Krebs, *J. Electrochem. Soc.* **2007**, *154*, B508.
[27] G. Munura, V. Rives-Arna, A. Saucedo, *J. Chem. Soc., Faraday Trans. 1* **1979**, *75*, 736.
[28] S. Guldin, S. Hüttner, P. Tiwana, M. C. Orilall, B. Ülgüt, M. Stefik, P. Docampo, M. Kolle, G. Divitini, C. Ducati, S. a. T. Redfern, H. J. Snaith, U. Wiesner, D. Eder, U. Steiner, *Energy Environ. Sci.* **2011**, *4*, 225.
[29] B. D. Cullity, *Elements of X-Ray Diffraction*, Addison-Wesley Publishing Company, Inc., Reading, Massachusetts **1956**.
[30] Y. B. Zheng, S. J. Wang, a. C. H. Huan, C. Y. Tan, L. Yan, C. K. Ong, *Appl. Phys. Lett.* **2005**, *86*, 112910.
[31] F. Huang, Y. Cheng, R. Caruso, *Aust. J. Chem.* **2011**, *6*, 820.
[32] H.-S. Lee, C.-S. Woo, B.-K. Youn, S.-Y. Kim, S.-T. Oh, Y.-E. Sung, H.-I. Lee, *Top. Catal.* **2005**, *35*, 255.
[33] L. Brus, *J. Phys. Chem.* **1986**, *90*, 2555.
[34] N. F. Mott, E. A. Davis, *Electronic Processes in Non-Crystalline Materials*, Oxford University Press, Oxford **1971**.
[35] F. Urbach, *Phys. Rev.* **1953**, *92*, 1324.
[36] R. Street, *Hydrogenated Amorphous Silicon*, Cambridge University Press, Cambridge UK **1991**.
[37] B. C. O'Regan, S. Scully, a. C. Mayer, E. Palomares, J. Durrant, *J. Phys. Chem. B* **2005**, *109*, 4616.
[38] D. Cuscn, P. Cells, B. C. O. Regan, F. Lenzmann, *Chem. Commun.* **2004**, 4342.
[39] E. Palomares, J. N. Clifford, S. a. Haque, T. Lutz, J. R. Durrant, *Chem. Commun.* **2002**, *14*, 1464.
[40] E. Palomares, J. N. Clifford, S. a. Haque, T. Lutz, J. R. Durrant, *J. Am. Chem. Soc.* **2003**, *125*, 475.
[41] A. Abate, T. Leijtens, S. Pathak, J. Teuscher, R. Avolio, M. E. Errico, J. Kirkpatrik, J. M. Ball, P. Docampo, I. McPherson, H. J. Snaith, *Phys. Chem. Chem. Phys.* **2013**, *15*, 2572.
[42] M. F. Yan, *J. Appl. Phys.* **1982**, *53*, 8809.
[43] D. Zhao, C. Chen, Y. Wang, W. Ma, J. Zhao, T. Rajh, L. Zang, *Environ. Sci. Technol.* **2008**, *42*, 308.

[44] M. M. Islam, T. Bredow, A. Gerson, *Phys. Rev. B* **2007**, *76*, 45217.
[45] P. R. F. Barnes, *Adv. Mater.* **2013**, *25*, 1881.
[46] J. M. Ball, M. M. Lee, A. Hey, H. J. Snaith, *Energy Environ. Sci.* **2013**, *6*, 1739.
[47] A. K. Ghosh, F. G. Wakim, R. R. Addiss, *Phys. Rev.* **1969**, *184*, 979.
[48] M. A. Henderson, *J. Sur. Sci.* **1999**, *419*, 174.
[49] M. Nolan, S. Elliott, J. Mulley, R. Bennett, M. Basham, P. Mulheran, *Phys. Rev. B* **2008**, *77*, 235424.
[50] S. Wendt, P. T. Sprunger, E. Lira, G. K. H. Madsen, Z. Li, J. Ø. Hansen, J. Matthiesen, A. Blekinge-Rasmussen, E. Laegsgaard, B. Hammer, F. Besenbacher, *Science* **2008**, *320*, 1755.
[51] N. A. Deskins, R. Rousseau, M. Dupuis, *J. Phys. Chem. C* **2010**, *114*, 5891.
[52] U. Diebold, *Surf. Sci. Rep.* **2003**, *48*, 53.
[53] E. Finazzi, C. Di Valentin, G. Pacchioni, A. Selloni, *J. Chem. Phys.* **2008**, *129*, 154113.
[54] G. Lu, A. Linsebigler, J. T. Yates, *J. Chem. Phys.* **1995**, *102*, 4657.
[55] J. Bisquert, A. Zaban, P. Salvador, *J. Phys. Chem. B* **2002**, *106*, 8774.
[56] J. Weidmann, T. Dittrich, *Sol. Energy Mater. Sol. Cells* **1999**, *56*, 153.
[57] Y. Yu, K. Wu, D. Wang, *Appl. Phys. Lett.* **2011**, *192104*, 2011.
[58] M. K. Akhtar, S. E. Pratsinis, *J. Mater. Res.* **1994**, *9*, 1241.
[59] A. Boronicolos, *J. Catalysis* **1986**, *68*, 59.
[60] J. Sasaki, N. L. Peterson, K. Hoshino, *J. Phys. Chem. Solids* **1985**, *46*, 1267.
[61] J. F. Stebbins, I. Farnan, U. Klabunde, *J. Am. Ceram. Soc.* **1989**, *200*, 2198.
[62] U. Gesenhues, T. Rentschler, A. O. Ti, P. Al Ti, *J. Solid State Chem* **1999**, *218*, 210.
[63] U. Gesenhues, *J. Photochem.Photobiol. A Chem.* **2001**, *139*, 243.
[64] J. A. S . Y. Chiang, B. D. Fabes, *J. Am. Ceram. Soc.* **1990**, *73*, 1633.
[65] C. R. A. Catlow, D. C. Sayle, P. Nortiers, *J. Phys. Chem. Solids* **1995**, *56*, 799.
[66] R. Shirley, M. Kraft, O. R. Inderwildi, *Phys. Rev. B* **2010**, *81*, 075111.
[67] S. Guldin, *Small* **2012**, *8*, 432.
[68] B. C. O'Regan, F. Lenzmann, *J. Phys. Chem. B* **2004**, *108*, 4342.
[69] Z. Bisquert, A. Juan, *J. Am. Chem. Soc.* **2004**, *126*, 13550.
[70] P. Docampo, S. Guldin, *Adv. Funct. Mater.* **2010**, *20*, 1787.